Screening single-atom catalysts for methane activation: α-Al_2O_3(0001)-supported Ni

Fei Gao,[1,2] Shiwu Gao,[1] and Sheng Meng[1,2,3,*]

[1]*Beijing Computational Science Research Center, Beijing 100193, China*

[2]*Beijing National Laboratory for Condensed Matter Physics, and Institute of Physics, Chinese Academy of Sciences, Beijing 100190, China*

[3]*Collaborative Innovation Center of Quantum Matter, Beijing 100190, China*

(Received 31 May 2017; published 24 August 2017)

Methane activation is one of the biggest challenges for chemical conversion of hydrocarbons and fundamental science. We systematically screen d-block transition metal elements as potential candidates of single-atom catalysts (SACs) for methane dissociation. The adsorption of methane on free metal atoms strongly depends on the number of d electrons of SAC, where the maximum binding energy is formed with the Ni group (electronic configuration d^8s^2 or d^9s^1). Interestingly, the magnetic moment of the SACs decreases by $2\mu_B$ for strong interactions, suggesting that the methane-metal bond forms a spin singlet state involving two electrons of opposite spins. To examine the effect of substrates, the screened transition metals, Ni, Rh, and Pt are further put onto prototype metal oxide surfaces. The substrate dramatically modifies the discrete energy levels of a single metal and its catalytic properties. Single Ni atoms supported on an O-terminated α-Al_2O_3(0001) surface (Ni_1/Al_2O_3) show superior catalytic properties, with a low activation barrier of 0.4 eV (0.11 eV after zero-point energy correction) for the C-H bond dissociation and simultaneously an extreme stability with a high binding energy of ~9.39 eV for the Ni anchor. This work identifies Ni_1/Al_2O_3 catalyst as an optimal SAC and offers new atomistic insights into the mechanism of methane activation on SACs.

DOI: 10.1103/PhysRevMaterials.1.035801

I. INTRODUCTION

A single metal atom, possessing the smallest size among all metallic nanoparticles and serving as an emerging type of heterogeneous catalysts, has been widely studied in the last five years [1–15]. As is well known the size of metal clusters is a key parameter in determining the performance of catalytic activities and reaction pathways. Noble metals like gold, which are inert in the bulk phase, become reactive in small size clusters. The increasing number of active sites of small nanoclusters and the quantized electron energy levels exhibit a distinctive gap between the highest occupied molecular orbital (HOMO) and the lowest unoccupied molecular orbital (LUMO), leading to dramatic quantum size effects. The effects become more prominent when the dimension is reduced down to a single atom. Single-atom catalysts (SACs) may offer great potential for high chemical activity and selectivity in many processes, e.g., water gas shift reaction. For instance, it was reported recently that a single-atom catalyst, Pt_1/FeO_x, was almost 2–3 times more active than other catalysts for CO oxidation, and at the same time exhibited excellent stability on iron oxide [10].

Among numerous chemical reactions, the activation of methane has always attracted great interests in fundamental and applied researches, driven by industrial needs and economic benefits [16–20]. Traditionally, planar and stepped nickel surfaces are the most commonly used catalysts for various practical processes such as Fischer-Tropsch (FT) synthesis and steaming methane reforming (SMR) [21–24], because of its low expenditure and acceptable reactivity. Noble metal surfaces, such as Rh and Pt, are also explored in theoretical studies and laboratory experiments, to promote the efficiency of reactions [25–27], for example, P. Bothra *et al.* reported that Rh(110) surfaces have a lower barrier of 0.69 eV than those on pure Ni(110) with a chemical barrier of 0.89 eV, for the first C-H bond cleavage [28]. It is, however, hard to find industrial applications due to the high cost and less availability of these metals. Moreover, the isolated and supported metal clusters, such as Au_2 [29] and Fe_2 [30], have also been considered as good candidates for methane activation. But their stability and reactivity are severely limited when used in a practical environment. Recently, SACs have also been proposed for the conversion of methane [31,32]. Using single iron atoms confined in silica (Fe©SiO_2), X.G. Guo *et al.* worked out a direct conversion of methane into high-value chemical products, especially ethylene and aromatics, without the production of carbon dioxide at 1636 K [33]. This may provide a new probable way to activate CH_4 molecules in spite of its high reaction temperature.

In the present work, we study systematically the activation of methane, in particular the adsorption and the C-H bond cleavage of CH_4($CH_4 \rightarrow CH_3 + H$) on free and supported single transition metals (TMs) using density functional theory (DFT). It is well known that methane molecule has a tetrahedral geometry and close shell electronic configuration without electronic and spin polarization. It has a strong C-H bond strength of 4.5 eV, making it thermodynamically stable in room temperature. The breaking of the first C-H bond is the initial and rate-limiting step of many reactions involving methane. On single $3d$, $4d$, or $5d$ TM atoms, the adsorption energy of methane is found to depend closely on the number of d electrons. The metal atom does not bind a CH_4 molecule if its d-orbital filling is empty, half- or full-filled; whereas strong interaction occurs when the number of d electrons is nearly full, e.g., on Ni, Pt, and Rh. This is mainly because the sp^3 orbitals of CH_4 prefer to interact with the d_z^2, d_{xz}, and d_{yz} orbitals of metals with favorable charge transfer from methane to TM atoms. When a much stronger carbon-metal

*Correspondence and requests for materials should be addressed: smeng@iphy.ac.cn

(C-M) bond is formed, the magnetic moments of the TM atoms decrease by $2\mu_B$, resulting in a large methane adsorption energy of ~0.3 eV. It also suggests the formation of a singlet spin state upon methane adsorption. After a primary screening, four SAC candidates, Ni, Pt, Rh, and Pd atoms are chosen for detailed investigation. The first three atoms display good catalytic capabilities for the C-H bond activation with almost vanishing dissociation barriers. To simulate more realistic catalysts, these single metal atoms, Ni, Pt, and Rh, are put onto α-Al_2O_3 surface, where the binding of the metal atoms and the dissociation barrier of methane are calculated. Single Ni atoms supported on O-terminated α-Al_2O_3(0001) surface (Ni_1/Al_2O_3) show not only a low-energy barrier of 0.4 eV for C-H bond cleavage, but also a large metal adsorption energy of 9.39 eV per Ni atom. It has the best stability and chemical reactivity for methane dissociation. Our calculations provide atomic level insights into the mechanism of methane activation on SACs, and identify the optimal Ni_1/Al_2O_3 catalyst for methane dissociation.

II. COMPUTATIONAL METHODS

Our first-principles calculations are performed within the framework of DFT using Vienna *ab initio* simulation package (VASP) [34]. The projector augmented wave (PAW) [35,36] pseudopotentials and the general gradient approximation (GGA) [37] in Perdew-Burke-Ernzerholf form [38] in all cases and the Bayesian error estimation functional with van der Waals correlation (BEEF-vdW) functional [39] in the cases of all free metal atoms and the Ni_1/Al_2O_3 catalyst for exchange-correlation energy are employed. A plane-wave cutoff of 400 eV is used to expand the wave function. Spin polarization is invoked in all calculations.

For the models of free single TM atoms, the supercell usually contains a vacuum layer of >15 Å and only one k point is used. All atoms are allowed to relax until the forces on each atom converge to less than 0.01 eV/Å. Furthermore, different initial configurations for each case are calculated and checked to ensure that the optimized geometry has the ground state spin configuration. The α-Al_2O_3 substrate is modeled by a 15 atomic layer slab with metal atoms sitting in a 2×2 supercell, corresponding coverage of 0.25 monolayer (ML) of metal atoms. The bottom three layers in the slab are fixed at their respective bulk position. The lattice constant of the Al_2O_3 slab is optimized to be 4.80 Å, consistent with the experimental value, 4.76 Å [40]. We consider the most stable facet (0001) using a vacuum layer of 20 Å along the z axis and the sampling of the Brillouin zone with a $3 \times 3 \times 1$ k-point grid. All atoms except those in the fifth trilayer of Al_2O_3 are allowed to relax until the force is less than 0.04 eV/Å. The dipole correction along the vertical direction is always included.

Reaction pathways are explored with the climbing image nudged elastic band (CI-NEB) method [41–43]. The initial and final state geometries for each step of all models are tested, and the ones with lowest energies are selected as the reactants and products in the minimum energy path (MEP). Our NEB calculations are considered converged when all forces are smaller than 0.01 and 0.1 eV/Å for the cases with isolated and supported metal atoms, respectively.

III. RESULTS AND DISCUSSION

A. Methane dissociation on isolated single metal atoms

It is well known that methane turns to be more active on transition metals, such as nickel. The first step of methane dissociation, $CH_4 \rightarrow CH_3 + H$, is generally considered as the rate-limiting step. We thus explore the adsorption and dehydrogenation of CH_4 molecule on an isolated TM atom with d electrons, as shown in Fig. 1. Calcium and zinc atoms are also included for comparison. The inset in Fig. 1 represents the thermodynamically preferred adsorption geometry of methane. Here, the adsorption energy of methane is given by the following formula:

$$E_{ads}^{CH_4} = E_{CH_4} + E_M - E_{CH_4\text{-}M}, \quad (1)$$

where E_{CH_4}, E_M, and $E_{CH_4\text{-}M}$ are the total energies of a CH_4 molecule, the single metal, and the complex of CH_4 and metal atom (CH_4-M), respectively. Considering the limitation of the pure GGA-PBE functional on methane adsorption, more accurate exchange-correction functional, the BEEF-vdW functional, is employed, and the GGA-PBE results are shown in Ref. [44], Fig. S1. It is obvious that all the Ca-, Sc-, Cu-, and Zn-group elements, whose d orbitals are either nearly zero or fully filled, bind weakly to CH_4 molecules with an adsorption energy less than 0.1 eV. The same trend also occurs for the half-filled d-orbital elements such as Cr, Mn, Mo, Tc, and Re. This weak binding is mainly generated by their stable d-electron configuration, which leads to an unfavorable charge transfer between methane and the metal atoms. In contrast, common catalysts, including the Ni-group elements and Rh atom, are more favorable for methane adsorption with the binding energies all larger than 0.2 eV, reaching even 0.46 eV for Rh and 0.49 eV for Pt as found in previous works [45,46]. The error estimations by this functional here are small, with an average value of 0.098 eV.

The calculated magnetic moments of free TM atoms with/without CH_4 molecule are also listed in Fig. 1. Upon methane adsorption, magnetic moment generally decreases by $2\mu_B$ for Ni, Rh, and Pt, suggesting a strong exchange coupling between CH_4 and the TM atoms, which implies that the CH_4 molecule is chemically adsorbed on such atoms. A covalent carbon-metal bond is formed involving a pair of electrons with opposite spins, shown in Fig. 2(a). The magnetic moment does not need to change for the Pd atom, where it is already in the spin singlet ground state.

It is interesting that single TM atoms with eight and nine d electrons, such as the Ni, Rh, Pt, and Pd atoms, have the strongest capability for methane adsorption with magnetic variation (adsorption energy in the range of 0.2–0.5 eV). From the charge density difference for the CH_4 adsorbed on these metals, we find that the charge transfer from methane to metal and formation of a strong adsorbate-metal bond occur, shown in Ref. [44], Fig. S2. Furthermore, the partial density of states (PDOS) displays that the orbitals of methane prefer to have strong interactions with the d_z^2, d_{xz}, and d_{yz} orbitals of single metals. After this initial screening, we choose Ni-group elements and Rh as primary candidates of SACs, which are subject to further studies for the first C-H bond cleavage of methane.

Element	Ca	Sc	Ti	V	Cr	Mn	Fe	Co	Ni	Cu	Zn
Conf.	$3d^04s^2$	$3d^14s^2$	$3d^24s^2$	$3d^44s^1$	$3d^54s^1$	$3d^54s^2$	$3d^64s^2$	$3d^74s^2$	$3d^94s^1$	$3d^{10}4s^1$	$3d^{10}4s^2$
$E_{ads}^{CH_4}$ (eV)	0.018	0.046	0.100	0.040	0.023	-0.002	0.003	0.252	0.283	0.026	-0.008
M_{gs} (μ_B)	0.0	1.0	2.0	5.0	6.0	5.0	4.0	3.0	2.0	1.0	0.0
M_{ads} (μ_B)	0.0	1.0	2.0	5.0	6.0	5.0	4.0	3.0	0.0	1.0	0.0
Err (eV)	0.073	0.084	0.113	0.234	0.049	0.072	0.028	0.160	0.159	0.068	0.075
Element	Sr	Y	Zr	Nb	Mo	Tc	Ru	Rh	Pd	Ag	Cd
Conf.	$4d^05s^2$	$4d^15s^2$	$4d^25s^2$	$4d^45s^1$	$4d^55s^1$	$4d^55s^2$	$4d^75s^1$	$4d^85s^1$	$4d^{10}5s^0$	$4d^{10}5s^1$	$4d^{10}5s^2$
$E_{ads}^{CH_4}$ (eV)	0.030	0.009	-0.009	0.179	0.012	0.102	0.110	0.462	0.219	0.029	0.027
M_{gs} (μ_B)	0.0	1.0	2.0	5.0	6.0	5.0	4.0	3.0	0.0	1.0	0.0
M_{ads} (μ_B)	0.0	1.0	4.0	5.0	6.0	5.0	4.0	1.0	0.0	1.0	0.0
Err (eV)	0.065	0.071	0.342	0.136	0.062	0.055	0.069	0.093	0.185	0.045	0.050

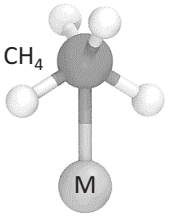

Hf	Ta	W	Re	Os	Ir	Pt	Au	Element
$5d^26s^2$	$5d^36s^2$	$5d^56s^1$	$5d^56s^2$	$5d^66s^2$	$5d^76s^2$	$5d^96s^1$	$5d^{10}6s^1$	Conf.
0.018	0.108	0.035	0.031	0.027	0.042	0.492	0.030	$E_{ads}^{CH_4}$ (eV)
2.0	3.0	6.0	5.0	4.0	3.0	2.0	1.0	M_{gs} (μ_B)
2.0	3.0	6.0	5.0	4.0	3.0	0.0	1.0	M_{ads} (μ_B)
0.065	0.089	0.047	0.055	0.067	0.089	0.136	0.088	Err (eV)

FIG. 1. The adsorption energy of methane on single metal atoms by the Bayesian error estimation functional with a van der Waals correlation (BEEF-vdW) functional. The electronic configuration and magnetic moment of metal atoms with/without CH_4 molecule are also summarized. The $E_{ads}^{CH_4}$ and Err represent the CH_4 adsorption energy and the Bayesian ensemble error, respectively. The inset shows the optimized geometry of the methane-metal atom complex (CH_4-M).

Although the CH_4 binding energy is over estimated generally and the magnetic moment of single Ti and V metal atoms and CH_4-Ru and CH_4-Ir complexes are not correct as shown in Ref. [44], Fig. S1, the pure GGA-PBE functional could give the same trends of methane adsorption on free TM atoms mentioned above. The optimized geometry and magnetic variation of methane on Pt, Rh, and Ni atoms are almost the same by the two functionals, shown in Table I and Fig. S1 in Ref. [44]. This is mainly because that the strong chemical interactions in such systems are dominant, and the GGA-PBE yields reasonable results for them. Based on this fact, we thus employ the GGA-PBE functional in the later studies, including the isolated and supported Pt, Rh and Ni atoms, and compare the results with those from the BEEF-vdW functional whenever necessary.

The calculated reaction barriers and optimized geometries of methane on the selected atoms are summarized in Table I. It can be seen that the Pt, Rh, and Ni atoms have small dissociation barriers (<0.1 eV), leading to an estimated

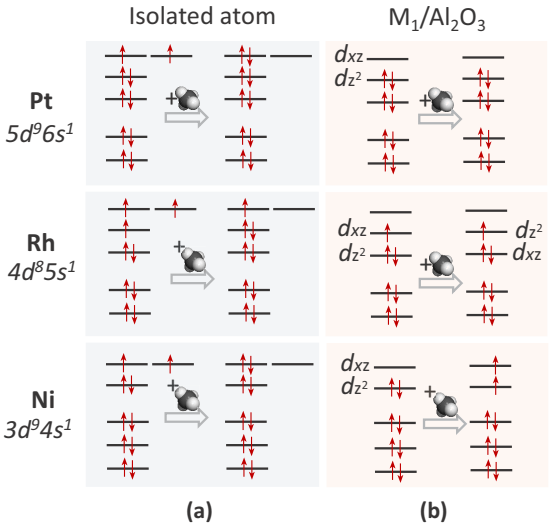

FIG. 2. Schematic illustration of orbital interactions of the Pt, Rh, and Ni atoms before and after methane binding for (a) isolated SACs and (b) those supported on Al_2O_3 substrate.

TABLE I. Chemical barriers for methane dissociation (E_B) and excess energy (E_{REST}) on four single metal atoms with GGA-PBE functional. Distances between carbon and metal in reactant ($d_{\mathrm{reactant}}^{CM}$) and product ($d_{\mathrm{product}}^{CM}$), and the angles between carbon, metal, and hydrogen ($\angle CMH$) are listed.

	E_B (eV)	E_{REST} (eV)	$d_{\mathrm{reactant}}^{CM}$ (Å)	$d_{\mathrm{product}}^{CM}$ (Å)	$\angle CMH$ (°)
Pt	0	1.33	2.10	1.97	95.3
Rh	0.06	0.67	2.20	1.98	93.0
Ni	0.09	0.31	1.91	1.84	94.7
Pd	0.35	−0.11	2.25	1.99	85.3

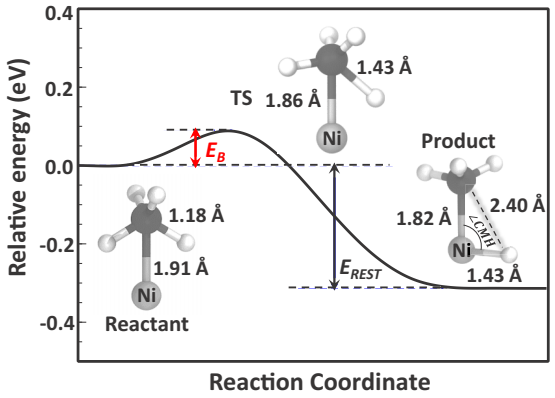

FIG. 3. Schematic representation of CH_4 dissociation reaction pathway on a single Ni atom by GGA-PBE functional. Optimized geometries of reactant, transition state (TS) and product are shown. Dark gray, white, and light gray spheres represent C, H, and Ni atoms, respectively. The E_B represents the reaction barrier and the E_{REST} stands for the excess energy.

reaction rate $\upsilon \approx 2.1 \times 10^{10}$ s^{-1} at room temperature (using a typical prefactor of 10^{12} s^{-1}). It means that conversion of a CH_4 molecule into the CH_3 and H fragments may be spontaneous. Our calculations also compare well with previous works [47,48]. For example, B. Liu *et al.* [48] reported that the binding energy of methane on single Ni atom is 0.4 eV with a reaction barrier of 1.7 kcal/mol (0.07 eV), which are similar to our results $E_{\mathrm{ads}}^{\mathrm{CH_4}} = 0.53$ eV and $E_B = 0.09$ eV, respectively. Moreover, the reaction barrier (0.12 eV), the excess energy (0.36 eV), and the optimized geometries of the reactant, transition state, and product for CH_4 on Ni atoms are almost the same if the BEEF-vdW functional is used, as shown in Ref. [44], Fig. S3, which indicates that GGA-PBE produces reasonable results. Comparing the three metals, a weak interaction between Pd and CH_4 molecules gives a higher chemical barrier of 0.35 eV. The excess energy denotes the potential energy difference between the product and reactant, given by the following formula:

$$E_{\mathrm{REST}} = E_{\mathrm{reactant}} - E_{\mathrm{product}}, \tag{2}$$

where E_{reactant} and E_{product} are the total energies of the reactants and products, respectively. For the Pd atom, the excess energy is -0.11 eV, which implies an irrationally thermodynamic activation for the C-H bond cleavage. Therefore we conclude Pd is not suitable for CH_4 activation and focus only on Pt, Rh, and Ni SACs below. Moreover, the adsorption of CH_4 molecules on Pt, Rh, and Ni atoms have similar structures for both the product and reactant by analyzing the distance between carbon and metal, and the angle between carbon, metal, and hydrogen ($\angle CMH$), as listed in Table I. The reaction pathway of methane activation on a free single Ni atom as an example is shown in Fig. 3, and the configuration of transition state is also close to that in earlier works [47,48]. Because of a favorable charge transfer from methane to the metals, the C-H bond of methane is greatly weakened on these three atoms, which leads to a much lower dissociation barrier of the CH_4 molecule, even 0 eV. Our results indicate that single TM atoms Ni, Rh, and Pt, are the most optimal candidates of catalysts for methane activation.

TABLE II. Metal binding energy (E_M) and methane adsorption energy ($E_{\mathrm{ads}}^{\mathrm{CH_4}}$) of Pt, Rh, and Ni atoms on MgO and Al_2O_3 surface with GGA-PBE functional.

		Al_2O_3(0001) (eV)		
	MgO(001) (eV)	Al-terminal surface	O-terminal surface	
	E_M	E_M	E_M	$E_{\mathrm{ads}}^{\mathrm{CH_4}}$
Pt	2.25	2.11	8.50	0.02
Rh	1.72	2.34	9.76	0.05
Ni	1.93	2.01	9.39	0.23

B. Methane activation on Ni_1/Al_2O_3(0001)

An ideal supporting substrate is vitally important for practical applications of SACs. It plays at least two significant roles here: one is to give prominence to catalysis by a suitable interaction between the single TM atoms and substrate; the other is to hold the single TM atoms tightly, in order to prevent aggregation of adsorbed metal atoms. It is, however, hard to keep a good balance between high catalytic activity and strong binding of metal atoms to the substrate. The dangling bonds of metal atoms would be saturated as the atom-substrate bonds are formed, often resulting in a weak interaction with methane molecules. Particularly, electronic states of metals could be modified and redistributed by the interactions between the substrates with TM atoms, which may result in quite different catalytic activation for methane molecules. Here, we explore the commonly used metal-oxide surfaces, such as MgO(001) and α-Al_2O_3(0001), as possible substrates to support single metal atoms [49,50]. All single TM atom adsorptions at the fcc, hcp, and bridge sites of the oxygen atoms in the top layer for both the O- and metal-terminated surfaces are considered. The distance between the neighboring metal atoms in adjacent supercells reaches 9.6 Å, which can be considered as isolated active sites in catalysis.

The adsorption energies of the Ni, Pt, and Rh atoms on three different substrates are listed in Table II. The O-terminated α-Al_2O_3(0001) surface exhibits an excellent capability for metal binding, with adsorption energies in the range of 8.5 to 9.76 eV per TM, which are much larger than the binding energies of $\sim$2.0 eV on the MgO(001) and the Al-terminated α-Al_2O_3(0001) surfaces. Importantly, these adsorption energies are also larger than the cohesive energies for bulk metals, which is on the order of 4.5 eV for bulk Ni. It means that the formation of metal clusters on an O-terminated α-Al_2O_3(0001) surface could be suppressed, otherwise the aggregation of metals would largely reduce the catalytic reactivity of SACs. Here, other phases of alumina such as γ-Al_2O_3 are excluded, due to their unsuitable geometries for catching single metal atoms [51,52]. It is noteworthy that the Al-terminated α-Al_2O_3(0001) surface in vacuum relaxes considerately with the cations moving toward the underlying anions, and has the lowest surface energy. This surface, however, is very reactive, and the terminal Al atoms can

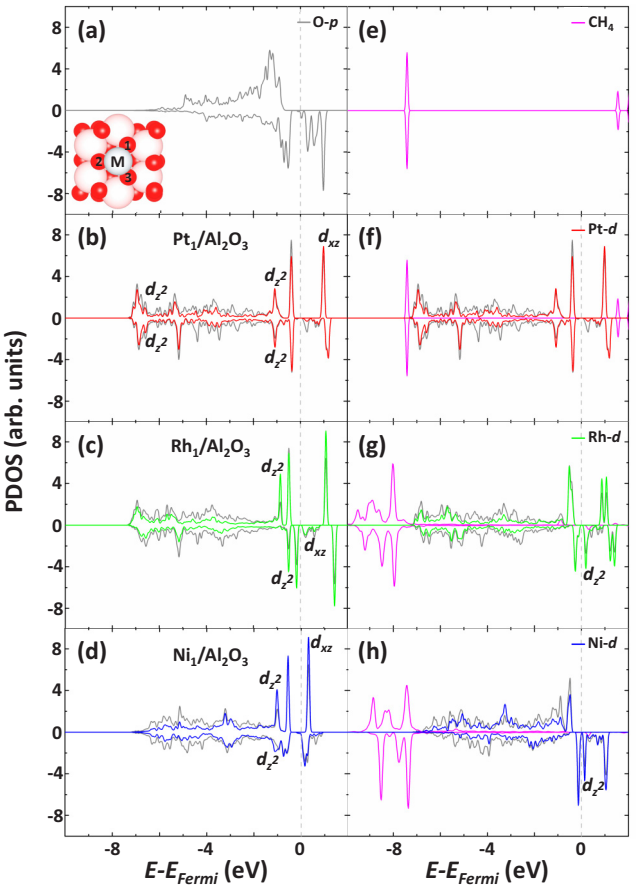

FIG. 4. Partial density of states (PDOS) projected onto the p orbitals of three adjacent oxygen atoms (gray lines) and d orbitals of Pt (red line), Rh (green lines), and Ni (blue lines) and CH_4 component (purple lines) in (a) clean O-terminated Al_2O_3; (b) Pt_1/Al_2O_3 catalyst; (c) Rh_1/Al_2O_3 catalyst; (d) Ni_1/Al_2O_3 catalyst; (e) free CH_4; and (f)–(h) CH_4 on M_1/Al_2O_3. The GGA-PBE functional is employed here. The inset displays the top view of M_1/Al_2O_3 catalyst, and metal and three adjacent oxygen atoms are all labeled. Pick, red, and light gray spheres represent Al, O, and metal atoms, respectively.

split water molecules to form solvated $Al(OH)_3$, which can be easily removed from the surface, leading to Al-deficient surfaces [53]. As a result, the O-terminated surface can be exposed to strongly bind metal atoms. In addition, a similar model catalyst, Pt_1/FeO_x, has been fabricated in experiment and used as an optimal single-atom catalyst for CO oxidation [10]. This is very similar to our model structure, in which each metal atom is embedded by three surface oxygen atoms. Moreover, O-terminated α-$Al_2O_3(0001)$ surfaces have been observed and investigated to illustrate the interactions with different metals [54]. With the development of experimental technology, the O-terminated metal substrates in catalysts have become more mature and popular.

Hereon, we consider single metal atoms embedded onto the O-terminated $Al_2O_3(0001)$ surface (M_1/Al_2O_3) as potential candidate SACs for methane activation with $M = \mathrm{Ni,Rh,Pt}$. Since the metal atom is bonded by three adjacent oxygen atoms on the surface [shown in the insert of Fig. 4(a)], the orbitals of the metal atom are now mostly occupied. Therefore smaller adsorption energies of methane on the O-terminated Al_2O_3 surface are expected than those on free atoms, also listed in Table II. Here, we focus on the electronic property and catalytic activation of M_1/Al_2O_3, beyond considering only the adsorption energy of methane. However, we note that at high temperatures, the lifetime of adsorption species decreases sharply during the activation of methane, and the adsorption-dissociation mechanism might transform to collision-dissociation pathways. An estimation of parameters on the adsorption or collision probability is also important, which is beyond the scope of the present study.

To our surprise, the adsorption of CH_4 on Ni_1/Al_2O_3 is relatively stable with an adsorption energy of 0.23 eV, which is substantially larger than that on Pt (0.02 eV) and Rh (0.05 eV) SACs. When using the BEEF-vdW functional, the adsorption energy of methane on Ni_1/Al_2O_3 is 0.33 eV with an error estimation of 0.196 eV. Detailed analysis of the hybridized energy states, as shown in Fig. 4, indicates that the CH_4-SAC interaction is dominated by the HOMO of the CH_4 and the d states of the SACs, namely the d_z^2, d_{xz}, and d_{yz} orbitals of TM atoms, around the Fermi level. According to the frontier molecule orbital (FMO) theory, the molecule adsorption energy depends on the difference between the HOMO-LUMO levels of the electron donor and acceptor. While the HOMO of CH_4 is the same in all cases, the empty d orbitals of the Ni atom lie 1 eV lower than that of the Pt and Rh, which explains a stronger CH_4 adsorption on Ni_1/Al_2O_3. This picture is also consistent with the d-band center theory that the higher energy position of the d-band center is more active in catalysis. In this case, the d-band center energy is $-5.62, -6.02$, and -6.25 eV for the supported Ni, Rh, and Pt, respectively.

Furthermore, the interaction between the CH_4 and the M_1/Al_2O_3 is dominated by the magnetic exchange interactions. The O-terminated α-$Al_2O_3(0001)$ surface is ferromagnetic with a magnetic moment of $1\mu_B$ for each dangling O bond on the surface. Metal adsorption removes the spin polarization of the three adjacent oxygen atoms, which dramatically reduces the magnetic moment (by $3-4\mu_B$) of the SACs. This reduction is mainly caused by the removal of surface symmetry breaking around the oxygen atoms. For methane adsorption, Figs. 4(f)–4(h), the magnetic moment increases by $4\mu_B$ on Ni_1/Al_2O_3, but does not change in the cases of Pt and Rh. For CH_4 on Ni_1/Al_2O_3, the spin-up part of the empty d orbitals is downshifted and becomes occupied. This shift of the spin-up state pushes the spin-down d_z^2 orbitals upwards, mediated likely by the on-site Coulomb correlation, and leads to the increase of the magnetic moment, as shown in Figs. 2(b) and 4(h). Such a spin interaction is also present in Rh SAC, but it does not change the local magnetic moment, keeping the magnetic moment of Rh $\sim 1\ \mu_B$. For the case of Pt, the interaction of the Pt d_z^2 orbitals with the O atoms is so strong that the Pt atom is fully saturated, leading to a much weaker interaction between methane and the Pt_1/Al_2O_3, as shown in Fig. 4(f). Figures 2 and 4 indicate the impact of exchange interaction on the catalytic behaviors of SACs, which is unknown before. It needs future experimental and theoretical attention.

Three additional systems, Ti_1/Al_2O_3, Ir_1/Al_2O_3, and Ru_1/Al_2O_3, are also studied, as shown in Ref. [44], Figs. S5

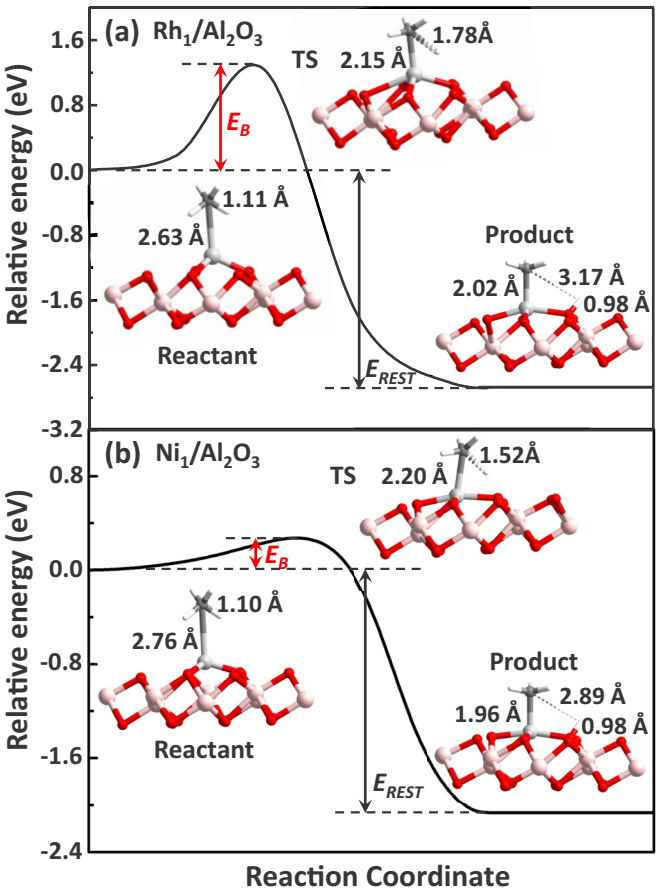

FIG. 5. Schematic representation of methane dissociation reaction pathway on (a) Rh_1/Al_2O_3 and (b) Ni_1/Al_2O_3 catalysts. The GGA-PBE functional is employed here. Optimized structures of reactants, transition states and products are all shown. Dark gray, white, light dark, red, and pink spheres represents C, H, Ni/Rh, O, and Al atoms, respectively. The E_B represents the reaction barrier and the E_{REST} stands for the excess energy.

and S6. The less d state of Ti near the Fermi level makes it hard to bind a CH_4 molecule. Like the case of Pt, due to strong interactions between the Ir dz^2 orbitals and the O atoms, Ir_1/Al_2O_3 catalysts have very weak interactions with methane. For Ru_1/Al_2O_3, methane adsorbs on metal with the binding energy of 0.03 eV, but the magnetic moment does not change. Figures S5 and S6 in Ref. [44] indicate that the empty spin-down d orbitals of Ru atom becomes occupied, and the spin-down dz^2 orbitals is upshifted, which is similar to Rh_1/Al_2O_3. Therefore the Ni_1/Al_2O_3 catalyst is the best one among all the supported SAC considered here.

Finally, NEB calculations have been performed to determine the MEP for methane activation on the Ni_1/Al_2O_3 catalyst. The reaction pathway on the Rh_1/Al_2O_3 catalyst is also given for comparison, as shown in Fig. 5. The structure of the reactants for both cases is rather similar, and the Ni and Rh atom tend to move from the fcc site to the nearby bridge site of the O atoms on the surface upon the CH_4 adsorption. Moreover, the excess energy of the Rh_1/Al_2O_3 catalyst is 0.56 eV larger than that on the Ni atom SAC, revealing the reaction with the Ni_1/Al_2O_3 catalyst is more favorable. The energy barrier on the Ni adsorbed surface is only 0.39 eV, which is 0.8 eV lower than that on Rh (1.2 eV). If the zero-point energy correction is considered during C-H bond cleavage, the barrier is further reduced from 0.39 to 0.11 eV (taken the half of CH vibration energy, 0.28 eV, as the zero-point energy). Here, the zero-point energy is calculated by taking the vibration frequency of the CH group $\tilde{v} \sim 2900\ \mathrm{cm}^{-1}$ into the following equation:

$$E_{\text{zero-point}} = \tfrac{1}{2}\hbar\omega = \tfrac{1}{2}hc\tilde{v}. \quad (3)$$

The low chemical barrier could make methane molecules cleave at room temperature. It is worth mentioning that a similar structure, γ-Al_2O_3 supported Ni_4 cluster, was reported as the catalyst for the first step of methane dissociation by J. Li *et al.* with a reaction barrier of 0.71 eV at interface sites [52]. This barrier is significantly larger than that for methane activation on SAC Ni_1/Al_2O_3 reported here. When comparing with an isolated Ni_4 cluster, the dissociation barrier of the first C-H bond on Ni_1/Al_2O_3 is still lower by 0.1 eV. Therefore we suggest that the single Ni atom adsorbed α-Al_2O_3 can be potential SAC for the methane activation, based on its overall structural stability and lower dissociation barrier.

In light of practical applications, it would be desirable to investigate further steps for integrated activation and convention of methane, such as SMR and formation of ethylene, because other steps can turn to be rate-limiting, even affecting the ability of the catalyst in different reactions. This is often related to the selectivity of the catalysts. For instance, the excess energy of 2.1 eV on Ni_1/Al_2O_3 at the initial step means the CH_3 group would rather dissociate to the CH_2 and H fragments than formation of ethylene with another CH_3 group. The results obtained in this work, however, offer new insights into the methane-metal interaction and mechanism of methane activation on SACs, which might be useful for many similar chemical processes. Using a different metal catalyst, the formation of ethylene could be favored by activating and combining two adjacent methane molecules. In addition, like most Ni/Al_2O_3 catalysts in general, the Ni_1/Al_2O_3 SAC can also deactivate due to possible $NiAl_2O_4$ formation and nickel sintering. This issue has been pursued in literature and is out of focus in the present study, which will be explored in future investigations.

IV. CONCLUSION

In summary, we systematically investigated single transition metal atoms as potential candidates for methane activation reactions based on extensive first-principles calculations. A preliminary screening on the CH_4 adsorption on isolated TM atoms identifies Ni, Rh, or Pt atoms as most promising SACs with large adsorption energy and magnetic change. The calculated activation barriers of methane are 0.09, 0.06, and 0 eV for Ni, Rh, and Pt, respectively. Furthermore, the stability and reactivity of the three selected metal atoms (Ni, Pt, Rh) supported on MgO(001) and α-Al_2O_3(0001) substrates are investigated. It is found that the O-terminated Al_2O_3(0001) surface possesses strong coupling with the metal atoms, leading to binding energies >9 eV. Moreover, the methane binding energy on supported single atoms is 0.23 eV for the Ni, 0.05 for Rh, and 0.02 eV for Pt, respectively. The PDOS analysis of the three atoms on the Al_2O_3 surface indicates that

the lowest empty d orbital of Ni atom is 1 eV lower than others, which is the main reason for their different capability towards methane adsorption. More importantly, the single Ni atom supported on O-terminated α-Al_2O_3(0001) surface also exhibits a low dissociation barrier of only 0.4 eV. The present work identifies therefore a novel single-atom catalyst Ni_1/Al_2O_3 and provides an atomic level insight into the mechanism of methane activation. This study offers an example for computational design of SACs and has broad implications.

ACKNOWLEDGMENTS

This work is partially funded by MOST (No. 2016YFA0300902 and 2015CB921001), China Postdoctoral Science Foundation (No. 2016M591056), and "Strategic Priority Research Program (B)" of the CAS (No. XDB07030100). We also acknowledge the allocated computer time at the supercomputer facility TH2-JK at the Beijing Computational Science Research Center (CSRC).

[1] G. Kyriakou, M. B. Boucher, A. D. Jewell, E. A. Lewis, T. J. Lawton, A. E. Baber, H. L. Tierney, M. Flytzani-Stephanopoulos, E. Charles, and H. Sykes, Science **335**, 1209 (2012).

[2] J. Lin, A. Wang, B. Qiao, X. Liu, X. Yang, X. Wang, J. Liang, J. Li, J. Liu, and T. Zhang, J. Am. Chem. Soc. **135**, 15314 (2013).

[3] X.-F. Yang, A. Wang, B. Qiao, J. Li, J. Liu, and T. Zhang, Acc. Chem. Res. **46**, 1740 (2013).

[4] S. Sun, G. Zhang, N. Gauquelin, N. Chen, J. Zhou, S. Yang, W. Chen, X. Meng, D. Geng, M. N. Banis, R. Li, S. Ye, S. Knights, G. A. Botton, T.-K. Sham, and X. Sun, Sci. Rep. **3**, 1775 (2013).

[5] Z.-Y. Li, Z. Yuan, X.-N. Li, Y.-X. Zhao, and S.-G. He, J. Am. Chem. Soc. **136**, 14307 (2014).

[6] J. Jones, H. Xiong, A. T. DeLaRiva, E. J. Peterson, H. Pham, S. R. Challa, G. Qi, S. Oh, M. H. Wiebenga, X. I. P. Hernández, Y. W., and A. K. Datye, Science **353**, 150 (2016).

[7] P. Liu, Y. Zhao, R. Qin, S. Mo, G. Chen, L. Gu, D. M. Chevrier, P. Zhang, Q. Guo, D. Zang, B. Wu, Gang Fu, and Nanfeng Zheng, Science **352**, 797 (2016).

[8] J. Ge, D. He, W. Chen, H. Ju, H. Zhang, T. Chao, X. Wang, R. You, Y. Lin, Y. Wang, J. Zhu, H. Li, B. Xiao, W. Huang, Y. Wu, X. Hong, and Y. Li, J. Am. Chem. Soc. **138**, 13850 (2016).

[9] W. Liu, L. Zhang, W. Yan, X. Liu, X. Yang, S. Miao, W. Wang, A. Wang, and T. Zhang, Chem. Sci. **7**, 5758 (2016).

[10] B. Qiao, A. Wang, X. Yang, L. F. Allard, Z. Jiang, Y. Cui, J. Liu, J. Li, and T. Zhang, Nat. Chem. **3**, 634 (2011).

[11] S. F. J. Hackett, R. M. Brydson, M. H. Gass, I. Harvey, A. D. Newman, K. Wilson, and A. F. Lee, Angew. Chem. Int. Ed. **119**, 8747 (2007).

[12] X. Zhang, J. Guo, P. Guan, C. Liu, H. Huang, F. Xue, X. Dong, S. J. Pennycook, and M. F. Chisholm, Nat. Commun. **4**, 1924 (2013).

[13] P. Hu, Z. Huang, Z. Amghouz, M. Makkee, F. Xu, F. Kapteijn, A. Dikhtiarenko, Y. Chen, X. Gu, and X. Tang, Angew. Chem. Int. Ed. **53**, 3418 (2014).

[14] Y.-G. Wang, D. Mei, V.-A. Glezakou, J. Li, and R. Rousseau, Nat. Commun. **6**, 6511 (2015).

[15] N. Cheng, S. Stambula, D. Wang, M. N. Banis, J. Liu, A. Riese, B. Xiao, R. Li, T.-K. Sham, L.-M. Liu, G. A. Botton, and X. Sun, Nat. Commun. **7**, 13638 (2016).

[16] F. Ancilotto, G. L. Chiarotti, S. Scandolo, and E. Tosatti, Science **275**, 1288 (1997).

[17] J. R. Rostrup-Nielsen, and J. K. Nørskov, Adv. Catal. **47**, 65 (2002).

[18] D. Schröder and H. Schwarz, PNAS **105**, 18114 (2008).

[19] D. Zhong, J. H. Franke, S. K. Podiyanachari, T. Blömker, H. Zhang, G. Kehr, G. Erker, H. Fuchs, and L. Chi, Science **334**, 213 (2011).

[20] A. A. Latimer, A. R. Kulkarni, H. Aljama, J. H. Montoya, J. S. Yoo, C. Tsai, F. Abild-Pedersen, F. Studt, and J. K. Nørskov, Nat. Mater. **16**, 225 (2017).

[21] J. Sehested, Catal. Today **111**, 103 (2006).

[22] E. Nikolla, J. Schwank, and S. Linic, J. Catal. **263**, 220 (2009).

[23] J. Li, E. Croiset, and L. Ricardez-Sandoval, App. Surf. Sci. **311**, 435 (2014).

[24] C. F. Huo, Y. W. Li, J. Wang, and H. Jiao, J. Am. Chem. Soc. **131**, 14713 (2009).

[25] J. Harris, J. Simon, A. C. Luntz, C. B. Mullins, and C. T. Rettner, Phy. Rev. Lett. **67**, 652 (1991).

[26] B. S. Bunnik and G. J. Kramer, J. Catal. **242**, 309 (2006).

[27] S. Nave, A. K. Tiwari, and B. J. Jackson, J. Chem. Phys. **132**, 054705 (2010).

[28] P. Bothra and S. K. Pati, Nanoscale **6**, 6738 (2014).

[29] S. M. Lang, T. M. Bernhardt, R. N. Barnett, and U. Landman, Angew. Chem. Int. Ed. **49**, 980 (2010).

[30] Q. Sun, Z. Li, A. Du, J. Chen, Z. Zhu, and S. C. Smith, Fuel **96**, 291 (2012).

[31] Y.-X. Zhao, Z.-Y. Li, Z. Yuan, X.-N. Li, and S.-G. He, Angew. Chem. Int. Ed. **53**, 9482 (2014).

[32] Y.-K. Li, Z. Yuan, Y.-X. Zhao, C. Zhao, Q.-Y. Liu, H. Chen, and S.-G. He, J. Am. Chem. Soc. **138**, 12854 (2016).

[33] X. Guo, G. Fang, G. Li, H. Ma, H. Fan, L. Yu, C. Ma, X. Wu, D. Deng, M. Wei, D. Tan, R. Si, S. Zhang, J. Li, L. Sun, Z. Tang, X. Pan, and X. Bao, Science **344**, 616 (2014).

[34] G. Kresse and J. Hafner, Phys. Rev. B **47**, 558 (1993).

[35] D. Vanderbilt, Phys. Rev. B **41**, 7892 (1990).

[36] P. E. Blöchl, Phys. Rev. B **50**, 17953 (1994).

[37] Y. Wang and J. P. Perdew, Phys. Rev. B **44**, 13298 (1991).

[38] J. P. Perdew, K. Burke, and M. Ernzerhof, Phys. Rev. Lett. **77**, 3865 (1996).

[39] J. Wellendorff, K. T. Lundgaard, A. Møgelhøj, V. Petzold, D. D. Landis, J. K. Nørskov, T. Bligaard, and K. W. Jacobsen, Phys. Rev. B **85**, 235149 (2012).

[40] D. Yang, M. Krasowska, R. Sedev, and J. Ralston, Phys. Chem. Chem. Phys. **12**, 13724 (2010).

[41] G. Mills, H. Jónsson, and G. K. Schenter, Surf. Sci. **324**, 305 (1995).

[42] G. Henkelman and H. Jónsson, J. Chem. Phys. **113**, 9978 (2000).

[43] G. Henkelman, B. P. Uberuaga, and H. Jónsson, J. Chem. Phys. **113**, 9901 (2000).

[44] See Supplemental Material at http://link.aps.org/supplemental/10.1103/PhysRevMaterials.1.035801 for adsorption energy and projected density of states of methane on single atoms in PBE; CH_4 reaction pathway on free Ni atom; charge density plot for methane on Ni_1/Al_2O_3; projected density of states for other SACs; and corresponding tables on adsorption energy and structural parameters.

[45] A. M. C. Wittborn, M. Costas, M. R. A. Blomberg, and P. E. M. Siegbahn, J. Chem. Phys. **107**, 4318 (1997).
[46] P. W. van Grootel, R. A. Santen, and E. J. M. Hensen, J. Phys. Chem. C **115**, 13027 (2011).
[47] H. Q. Yang, Y. Q. Chen, C. W. Hu, M. C. Gong, H. R.Hu, A. M. Tian, and N. B. Wong, Chem. Phys. Lett. **355**, 233 (2002).
[48] B. Liu, M. T. Lusk, and J. F. Ely, J. Phys. Chem. C **113**, 13715 (2009).
[49] J. W. Elam, C. E. Nelson, M. A. Cameron, M. A. Tolbert, and S. M. George, J. Phys. Chem. B **102**, 7008 (1998).
[50] J. H. Kwak, J. Hu, D. Mei, C.-W. Yi, D. H. Kim, C. H. F. Peden, L. F. Allard, and J. Szanyi, Science **325**, 1670 (2009).
[51] M. Sun, A. E. Nelson, and J. Adjaye, J. Phys. Chem. B **110**, 2310 (2006).
[52] J. Li, E. Croiset, and L. Ricardez-Sandoval, J. Phys. Chem. C **117**, 16907 (2013).
[53] G. Carchini, M. García-Melchor, Z. Łodziana, and N. López, Appl. Mater. Interfaces **8**, 152 (2016).
[54] J. Rosén, J. M. Schneider, and K. Larsson, J. Phys. Chem. B **108**, 19320 (2004).